Title
Natural Neural Projection Dynamics Underlying Social Behavior

Journal
Cell, 157(7)

ISSN
0092-8674

Authors
Gunaydin, Lisa A
Grosenick, Logan
Finkelstein, Joel C
et al.

Publication Date
2014-06-01

DOI
10.1016/j.cell.2014.05.017

Peer reviewed

Published in final edited form as:
Cell. 2014 June 19; 157(7): 1535–1551. doi:10.1016/j.cell.2014.05.017.

Natural neural projection dynamics underlying social behavior

Lisa A. Gunaydin[1,*], **Logan Grosenick**[1,2,*], **Joel C. Finkelstein**[1,*], **Isaac V. Kauvar**[1,*], **Lief E. Fenno**[1,2], **Avishek Adhikari**[1], **Stephan Lammel**[3], **Julie J. Mirzabekov**[1], **Raag D. Airan**[1], **Kelly A. Zalocusky**[1,2], **Kay M. Tye**[1], **Polina Anikeeva**[1], **Robert C. Malenka**[3], and **Karl Deisseroth**[1,3,4,6]

[1]Department of Bioengineering, Stanford University, Stanford, CA

[2]Neuroscience Program, Stanford University, Stanford, CA

[3]Department of Psychiatry and Behavioral Sciences, Stanford University, Stanford, CA

[4]Howard Hughes Medical Institute, Stanford University, Stanford, CA

Abstract

Social interaction is a complex behavior essential for many species, and is impaired in major neuropsychiatric disorders. Pharmacological studies have implicated certain neurotransmitter systems in social behavior, but circuit-level understanding of endogenous neural activity during social interaction is lacking. We therefore developed and applied a new methodology, termed fiber photometry, to optically record natural neural activity in genetically- and connectivity-defined projections to elucidate the real-time role of specified pathways in mammalian behavior. Fiber photometry revealed that activity dynamics of a ventral tegmental area (VTA)-to-nucleus accumbens (NAc) projection could encode and predict key features of social but not novel-object interaction. Consistent with this observation, optogenetic control of cells specifically contributing to this projection was sufficient to modulate social behavior, which was mediated by type-1 dopamine receptor signaling downstream in the NAc. Direct observation of projection-specific activity in this way captures a fundamental and previously inaccessible dimension of circuit dynamics.

INTRODUCTION

Impaired social interaction is a hallmark of several psychiatric disorders including autism, schizophrenia, depression, and social anxiety disorder. In rodents, most studies on social behavior have focused on socio-sexual behaviors, such as pair bonding and behaviors related to sexual competition (Aragona et al., 2006; Curtis and Wang, 2005; Gingrich et al., 2000; Leypold et al., 2002; Liu and Wang, 2003; Young et al., 2001; Young and Wang, 2004). However, comparatively little is known about neural circuitry regulating adult same-sex, non-aggressive social interaction, which is of potential relevance for understanding circuits that go awry in social-function disorders (Silva and Ehninger, 2009).

[6]To whom correspondence should be addressed: Karl Deisseroth, M.D., Ph.D., Department of Bioengineering, W083 Clark Center, 318 Campus Drive, Stanford, CA 94305, Phone: (650) 736-4325, deissero@stanford.edu.
*authors contributed equally

Pioneering studies have implicated the neuromodulator dopamine (DA) in same-sex affiliative interactions (Puglisi-Allegra and Cabib, 1997; Robinson et al., 2002; Robinson et al., 2011). DA neurons in the VTA are involved in processing emotionally salient stimuli of both positive and negative valence. The VTA is a heterogeneous region comprised of diverse cell types which may play distinct roles in modulating reward and aversion based on connectivity to different upstream and downstream structures (Brischoux et al., 2009; Budygin et al., 2012; Chaudhury et al., 2013; Kalivas and Nakamura, 1999; Lammel et al., 2011; Lammel et al., 2012; Mirenowicz and Schultz, 1996; Tye et al., 2013). These cells project broadly throughout the brain to limbic regions such as the medial prefrontal cortex (mPFC), NAc, and amygdala, structures that may mediate both appetitive and aversive processes. However, it is unknown which if any of these projections might play a causal role in driving or inhibiting social behaviors. Moreover, in general the real-time neural circuit dynamics causally involved in social behavior remain poorly understood, and the large number of downstream VTA targets and postsynaptic DA receptors together point to the need for new tools that allow observation of targeted cell types and their projections during naturalistic conditions, and perturbation of activity in a downstream receptor and region-specific manner.

We approached this challenge by developing optical tools to selectively observe and control specific VTA circuit elements, projections, and downstream targets on a timescale relevant to social interaction. First we sought to develop a recording technique sensitive enough to track real-time dynamics of genetically and topologically specified subsets of neuronal projections in freely moving mice, using novel photometric devices together with genetically-encoded Ca^{2+} indicators (Akerboom et al., 2012; Chen et al., 2013) for direct *in vivo* measurement of a previously-inaccessible variable: the coordinated activity of neuronal afferents projecting to a particular downstream target in the brain of a behaving animal. We next applied this method to determine quantitative features of projection-specific dynamics during behavior, to identify circuit elements predictive of social interactions. Complementing observation of these natural behaviorally-evoked activity patterns, we employed optogenetic tools to define causal roles of these same projections (relative to other pathways) in modulating social behavior. And finally, we engineered a light-activated postsynaptic neurotransmitter receptor to test the causal sufficiency of DA receptor signaling at the identified projection target for social behavior modulation. Together these investigations provide insight into natural and causal circuit dynamics underlying social behavior modulation, and illustrate an approach for testing the behavioral relevance of circuits characterized by cell location, type, projection target, and target receptor during behavior.

RESULTS

Optical detection of reward-related VTA Ca^{2+} signals in freely moving animals

Fast-scan cyclic voltammetry has revealed DA changes in striatal regions that correlate with bouts of social interaction (Robinson et al., 2002; Robinson et al., 2011). However, causality and specificity for cells or projections in driving social interaction have been unknown, and there have been no recordings of identified DA neurons or their projections during any social paradigm. To observe the real-time activity of specified neural projections in complex behaviors, we developed a novel technique, fiber photometry. Previous pioneering devices used multiple fiberoptics to record genetically-encoded Ca^{2+} signals in cell bodies of awake animals in striatum (Cui et al., 2013) and in cortex (Lutcke et al., 2010; Schulz et al., 2012). We developed a design that was simple (only a single multimode optical fiber), suitable for recording from deep brain structures, and sensitive enough to detect activity changes not only in cell bodies but also in axons during behavior, where signals are considerably smaller. This fiber photometry (light measurement with a single-fiberoptic device sensitive enough to detect activity in axonal fibers) relies on a lock-in amplifier and a high-sensitivity photoreceiver along with custom software to record (through an implanted 400 μm optical fiber) the population activity of neural circuit elements expressing a genetically encoded Ca^{2+} indicator (Fig. 1A). The single fiber allows chronic, stable, minimally disruptive access to deep brain regions, and interfaces with a flexible patchcord on the skull surface. For cell type-specific recording of Ca^{2+} transients—a proxy for certain neural activity (Akerboom et al., 2012)—we injected a Cre-dependent adeno-associated virus (AAV) carrying the GCaMP5g gene into VTA of transgenic TH::Cre mice (henceforth referred to as TH-GCaMP, Fig. 1A, Fig. S1A), and implanted an optical fiber in VTA for simultaneous delivery of 473 nm excitation light and collection of GCaMP5g fluorescence emission. Activity-dependent fluorescence emitted by cells in the volume is collected simultaneously; after propagating back through the same patchcord used to deliver excitation light, this fluorescence is spectrally separated using a dichroic, passed through a single band filter, and focused onto a photodetector (Fig. 1A).

To first test if this system were capable of detecting VTA activity in a temporally precise manner, we recorded Ca^{2+} signals in VTA neurons of TH-GCaMP mice given access to sucrose solution, an established natural reward. Sucrose consumption was assessed using a contact “lickometer”, which registered an event every time the mouse completed a circuit from a metal spout to a metal operant chamber floor, time-locked to the Ca^{2+} recording. This setup enabled readout of VTA response with temporal precision on the order of milliseconds. We observed a robust increase in VTA GCaMP fluorescence when mice licked for sucrose (average peak dF/F: 68.3% +/− 13.2% SEM; average mean dF/F: 29.7% +/− 8.9% SEM), an effect that was absent in control mice expressing eYFP (Fig. 1B). VTA signals were tightly correlated in time with onset of licking bouts (Fig. S1B), and habituated over recording epochs (Fig. S1C). While no driver-line or injection targeting is fully-specific, together with previous validation of high-specificity Cre expression in TH neurons of lateral VTA in this TH::Cre mouse line (Tsai et al., 2009; Tye et al., 2013) and DA receptor blockade results presented below, these data suggest validity of fiber photometry for recording temporally-precise behavior-related signals in the targeted population (here referred to as VTA-DA neurons).

Neural activity that encodes and predicts social interaction

Next we applied fiber photometry during same-sex social interaction. We recorded from the VTA of female mice during home-cage social interaction, in which a novel social target mouse was introduced into the test mouse cage for a 5 minute epoch, and video time-locked to the VTA GCaMP signal was collected. Upon introduction of the social target, we observed a marked increase in activity of the targeted VTA neurons during interaction with this novel mouse (Fig. 1C). This activity habituated over the behavior epochs, with strongest activity occurring during earlier bouts of interaction (Fig. 1D). Such activity was absent in the eYFP control, indicating that observed transients were Ca^{2+} signals and not motion artifacts (Fig. 1D).

To dissociate social activity from general novelty-related activity, in separate trials we exposed test mice to a novel object placed in the home cage (counterbalanced with novel-mouse exposure). Mice interacted more frequently with a stranger mouse than with a novel object (Kaplan-Meier estimate for latency to next interaction, log-rank test $p<0.0001$). Nevertheless, VTA activity in response to the novel object (Fig. 1E) resembled peak VTA activity during social interaction, with similar amplitude (mean peak dF/F during interaction: 16.4% +/− 2.1% SEM for social, 13.7% +/− 1.4% SEM for novel object, n=10; Wilcoxon signed-rank test, p=0.5; Fig. 1F) and similar decay across interaction epochs (peak fluorescence fit to e^{-kb}: k=decay rate and b=bout number; social: k=0.71, r^2=0.95, novel object: k=1.29, r^2=0.94; Fig. 1G). However, while social VTA responses aligned well with onset of interaction, novel object responses aligned more significantly with termination of the interaction bout (peak fluorescence within 0.5 s from end of interaction – peak fluorescence within 0.5 s from start: −1.7% dF/F for social, 9.7% dF/F for novel object; n=10 animals, Wilcoxon signed-rank test: p=0.0051; Fig. 1H), suggesting that VTA responses in these two behaviors could represent different information given distinct timing relative to interaction onset.

To more closely examine VTA representation of social and object interactions, we identified the peak fluorescence within each interaction epoch and segmented time-locked behavioral videos into 1 sec clips centered upon the time of maximal VTA activity to assess specific actions when VTA activity was highest. Behavior during these 1 sec segments was assigned a binary value for approach, withdrawal, or active investigation (contact). We found prominent differences in distribution of these behaviors in the social compared to novel object setting; when fluorescence was highest, mice exhibited significantly more withdrawals from the target during novel object epochs compared to social epochs (Fig. 1I; n=10, Wilcoxon rank-sum test with continuity correction, W=89, p=0.003). Conversely, peak fluorescence during social epochs was associated with significantly more approach behavior and active investigation than with novel object (Fig. 1I; n=10, Wilcoxon rank-sum test with continuity correction, W=10, p=0.0007 and W=0, p=0.0001, respectively; see also Fig. S1D). These data suggest that for social interaction, peak activity in these cells encodes appetitive approach behaviors, whereas during novel object investigation, peak activity appears to encode withdrawal behaviors.

Given the reliable association between peak VTA activity and approach/investigation of social targets, we hypothesized that observed DA neuron activity during a particular interaction epoch might be meaningful to the animal in terms of modulating its subsequent social approach behavior. To test this hypothesis we investigated whether magnitude of the VTA signal during one interaction bout would predict latency to engage in another social interaction bout. We employed prediction analysis, using peak Ca^{2+} activity (log-transformed; Methods) during one interaction to predict latency to engage in the next interaction. A survival regression model appropriate for time-to-event data was used to predict latency to the next interaction as a function of three variables: (1) peak Ca^{2+} activity (log-transformed), (2) time since target introduction (to control for habituation unrelated to neural activity), and (3) animal identity (to control for interanimal differences). For social interactions, increased peak Ca^{2+} activity during the previous interaction predicted shorter latency to interact again ($Z=-5.21$, $p<0.0001$), while time since target introduction instead predicted longer latency to interact ($Z=5.29$, $p<0.0001$; consistent with decreases in interaction over time typically observed in such data). However, peak Ca^{2+} activity did not predict reduced latency to novel object interactions, but instead showed a less pronounced effect in the opposite direction (significantly predicting longer latencies to the next interaction: $Z=1.19$, $p=0.02$; with a trend toward effect of time elapsed: $Z=0.475$, $p=0.053$). These data together illuminate the real-time dynamics of VTA-DA neurons during social interaction, demonstrating that activity of these neurons can predict social and novel object interaction behavior on a trial-by-trial basis, and that the direction of these predictions is opposite for the two types of interaction.

Prediction analysis suggested an important role for VTA-DA neuron activity in social interaction; however, since VTA-DA neuron activity and latency to social interaction are both correlated with time-elapsed from target introduction, we sought to further confirm that this predictive capability of the native dynamics of DA neurons on behavior was not merely mediated by the parameter of time elapsed. We used causal mediation analysis (Imai et al., 2010) to take into account effects of time elapsed on both VTA activity and behavior, represented by a simple directed graphical model (Fig. 1; Methods). If apparent effects of VTA-DA neuron activity on subsequent behavior were spurious, and time elapsed the only causal contributing influence to observed changes in latency to engage in interaction, we would expect time elapsed to completely mediate the effect of VTA-DA activity on this behavior. We found that while time elapsed partially mediated effects of VTA-DA neuron activity on latency to social interaction, the majority of the effect of VTA-DA neuron activity was direct rather than mediated (Fig 1J; 74.0% average direct effect, 26.0% average indirect effect mediated by time elapsed; both $p<0.0001$). In contrast, a similar mediation analysis on novel object interactions did not show significant direct or indirect effects of VTA-DA neuron activity on latency to interact (Fig 1J). Together these fiber photometry results indicate that native VTA-DA neural activity both encodes and predicts social interaction, and suggest that endogenous VTA dynamics may have a direct effect on social approach behavior.

Direct control of VTA-DA cells bidirectionally modulates social behavior

If VTA-DA activity peaks were causally involved in initiating or maintaining social interaction, then experimentally providing these otherwise rapidly-habituating signals could increase the overall amount of social interaction. To test this hypothesis, we selectively expressed a channelrhodopsin in VTA-DA neurons by injecting a Cre-dependent AAV encoding ChR2 fused to EYP (ChR2-eYFP) into VTA of TH::Cre mice (TH-ChR2, Fig. 2A), an approach previously shown to target DA neurons in the same region of lateral with >98% specificity (Tsai et al., 2009). TH-positive neurons showed robust ChR2 expression (Fig. 2B) and reliable elicitation of action potentials using 5 msec pulses of 473 nm light

(Fig. 2C). To assess the contribution of these neurons to social behavior, we employed the home cage social interaction assay (with novel-object control) as for fiber photometry, in which test mice in the home cage were separately exposed to two different stranger mice, one of which was paired with optical stimulation of VTA (counter-balanced for order of stimulation). Stimulation was delivered in 30 Hz bursts of light (8 pulses, 5 msec each; Fig. 2D) every 5 sec throughout the assay, a phasic pattern shown to evoke high levels of DA release (Adamantidis et al., 2011; Tsai et al., 2009). We then compared total time spent in active investigation between light off and light on epochs; scoring was conducted blind to genotype.

Phasic stimulation significantly increased investigation of the novel mouse, with no effect on controls (Fig. 2E; n=17 ChR2, n=18 eYFP, LME model, t_{57}=2.31, p=0.03; similar pro-social effects were also observed in male-male interactions, n=12, p=0.02, data not shown). To test whether VTA-DA cells were not only sufficient to increase social behavior but also necessary for full expression of social behavior, we inhibited VTA-DA neurons using eNpHR3.0 and found a significant decrease in social interaction (Fig. 2E; n=10 eNpHR3.0, n=15 eYFP, LME model, t_{57}=−2.09, p=0.04). These same conditions of VTA stimulation and inhibition had no effect on investigation of a novel object (Fig. 2F, Wilcoxon signed-rank test, p=0.41) or locomotion (Fig. S2, Wilcoxon signed-rank test, p=0.85). Together these optogenetic data demonstrate that phasic activity of VTA-DA neurons is sufficient to drive social interaction, and that inhibiting activity in this population impairs normal social behavior.

The observed selective influence of experimentally-modulated VTA-DA activity on social (but not novel-object) behavior contrasts with the apparent similarity of naturally-occurring VTA-DA activity peak magnitudes during social and novel-object interactions. Given similar VTA-DA activity peak magnitudes in the two behaviors, it could be that precise timing of delivered activity is relevant (without which the causal impact is not seen), or that naturally-occurring VTA-DA activity peaks are present in, but do not causally drive, the novel-object behavior. Indeed the activity peaks may be only superficially similar in the two cases; a causally-relevant subpopulation of VTA-DA neurons (not resolved by VTA photometry) could be driving social behavior. Even among cells that share the same physical location and genetic type, causally-relevant subpopulations may be present that are differentially connected (e.g. Warden et al., 2012) in a way that is resolvable by projection targeting; we thus next sought to identify and probe not only causal sufficiency, but also native predictive activity, of candidate projection populations during freely-moving behavior.

Activation of VTA-NAc but not VTA-mPFC projections favors social behavior

To guide these efforts, we sought to systematically identify candidate downstream projection targets. We began with a brainwide survey of VTA optogenetic stimulation-evoked induction of cFos, a marker of prolonged neural activity elevation (Fig. 3A,B). We found upregulation of cFos in NAc (Fig. 3C,D) and mPFC (Fig. 3E,F) but not in basolateral amygdala (BLA; Fig. 3G,H; n=4 ChR2, n=4 eYFP; t-test, NAc: p=0.00006, mPFC: p=0.002, BLA: p=0.82). With the resulting knowledge that NAc and mPFC were recruited by precisely the same optogenetic stimulation that increased social behavior (Fig. 2), we next carried out optogenetic targeting of VTA cells projecting to each of these two regions in social interaction. We injected the same Cre-dependent ChR2 virus into VTA, but targeted the optical fiber to either NAc or mPFC to activate VTA axons within these regions. Activation of cells with VTA-to-NAc projections (Fig. 4A) sufficed to increase social interaction (Fig. 4B, n=11 ChR2, n=12 eYFP, LME model, t_{30}=7.11, p=0.039) without affecting locomotion or novel object investigation (Fig. S3 A,B; Wilcoxon signed rank test, p=0.62 and p=0.63, respectively). Activation of the VTA-mPFC projection (Fig. 4C), on the other hand, had no effect on social interaction (Fig. 4D; n=7 ChR2, n=7 eYFP, LME model, t_{12}=0.11, p=0.39). This mPFC projection might instead be relevant in part to behavioral responses of negative valence, as mPFC-projecting VTA DA neurons respond *ex vivo* to potentially aversion-related stimuli (Lammel et al., 2011). Indeed, we found that driving the VTA-mPFC projection was sufficient to account for anxiety-like effects of direct VTA stimulation (Fig. S3 C–F, n=17 ChR2, n=18 eYFP, p=0.01 for cell bodies; n=7 ChR2 and n=7 eYFP, p=0.02 for mPFC projection), and sufficed to cause conditioned place aversion (Fig. S3 G–I, n=12 ChR2, n=14 eYFP, Wilcoxon signed rank test, p=0.02), highlighting the functional specificity of distinct VTA projections.

Although the subpopulation of VTA neurons projecting to NAc sufficed to mediate pro-social effects of VTA stimulation, NAc-terminating VTA axons were not distinguished from possible axons passing through the NAc. To address this question, we injected Cre-dependent DIO-ChR2 AAV into VTA of wild-type mice, and AAV carrying a wheat germ agglutinin (WGA)-Cre recombinase fusion, which crosses trans-cellularly into local axon terminals and is transported to upstream somata (Dong et al., 2011; Yuan et al., 2011), into medial NAc (Fig. 4E). With this approach (previously used to retrogradely target circuits; Gradinaru et al., 2010; Xu and Sudhof, 2013) ChR2 is targeted to the subpopulation of VTA cells terminating in NAc. With fiberoptic placement directly above VTA (Fig. 4F), we found that activation of cells with this connectivity sufficed to increase social interaction (Fig. 4G, n=14 ChR2, n=11 eYFP, t_{23}=2.53, p=0.02) without affecting locomotion or novel object investigation (data not shown; Wilcoxon signed rank test, p=0.85 and p=0.53, respectively). This approach gave sparse but strong expression of ChR2 in VTA, and selective expression of ChR2 in fibers in NAc but not mPFC or BLA (Fig. 4H), supporting previous findings that VTA subpopulations projecting to these regions are non-overlapping (Lammel et al., 2008) and indicating that behavioral effects are not attributable to antidromic spike propagation to collateral projections toward mPFC or BLA. Together, these results demonstrate that driving activity in VTA-NAc projections is sufficient to increase social interaction. Figure 4I summarizes behavioral effects of all VTA optogenetic interventions, illustrating the increasingly robust pro-social effect resulting from more projection-specific interventions.

Elevated NAc activity in pro-social optogenetic control and native social behavior

We examined expression of these social behavior-related activity processes in NAc, using electrophysiology both in the anesthetized state and in freely-moving animals during social interaction. First, during optogenetic stimulation in VTA of anesthetized animals, we observed increases in NAc firing (Fig. 5A – C): ~2-fold increased multiunit activity over several seconds following the VTA burst, and an even larger increase close to the burst itself (Fig. 5B,C; $p<0.001$), consistent with timescales expected from DAergic neuromodulation.

We next investigated NAc activity during social behavior. Further supporting this link, we found that brief social interaction led to robust cFos induction in NAc (Fig. 5D; $p=0.027$). Next, we implanted TH-ChR2 animals with an optical fiber in VTA and a 16-electrode recording array in NAc; recording from awake animals alone in the home cage, we observed a consistent light-evoked increase in NAc firing during optical drive of VTA-DA neurons comparable to that observed in anesthetized animals (Fig. S4). To determine whether NAc cell firing naturally increased when animals engaged in social interaction, we recorded during exploration of an apparatus consisting of a chamber containing a stranger conspecific, and an otherwise identical neutral chamber (Fig. 5E). This behavioral setting combined with video tracking allowed for temporally precise correlation of neural activity with defined social and neutral zones. We found that NAc multiunit activity was significantly higher when the test mouse was exploring the social chamber compared to the neutral chamber (Fig. 5G,H; $p=0.025$). Consistent with this increase in NAc firing during social behavior, bidirectional optogenetic modulation of VTA-NAc circuit elements (which modulated NAc firing in anesthetized and awake animals) produced the same bidirectional effects on social behavior in the three-chamber apparatus as in the home cage social assay (Fig. S4).

Detection of native VTA→NAc activity in social but not novel-object interaction

While these data were consistent with hypothesized importance of the VTA-NAc projection in social behavior, direct observation of endogeneous activity in the projection during social behavior remained lacking. This would require measuring a previously inaccessible but fundamental neural circuit quantity: native activity in a specific projection during behavior. Fiber photometry (Fig. 1) was designed for this technical challenge, and we next tested real-time tracking of Ca^{2+} transients in genetically-specified VTA inputs to NAc. Using TH-GCaMP mice, we implanted an optical fiber in medial NAc to detect activity specifically in axon fibers corresponding to the projection in question (Fig. 6A), during home cage social interaction and novel object investigation (Fig. 6B).

We observed robust GCaMP signals across many social interaction bouts, demonstrating that fiber photometry can be used to selectively record from neuronal projections (Fig. 6B,C) during behavior. We observed smaller projection activation to novel object (Fig. 6C,D; $n=11$, Wilcoxon signed rank test, mean peak dF/F: 6.9% +/− 1.4% for social, 3.5% +/− 0.7% for novel object, $p=0.016$). Moreover, decay kinetics of social and novel peaks across bouts were different (fitting peak fluorescence to e^{-kb} as before; novel object: $k=0.00$, $r^2=0.60$, social: $k=0.25$, $r^2=0.80$, Fig. 6E), as were peak fluorescence distributions between social and novel object conditions (log-rank test: $p=0.004$, $n=208$ social; $n=94$ object). Stronger encoding of social than object interactions by the VTA-NAc projection (not seen at the cell bodies) supports the hypothesis that there are distinctly-wired relevant subpopulations of VTA neurons. This conclusion was further supported by prediction and causal mediation analyses (as above for cell bodies). Peak Ca^{2+} activity during social interaction again predicted shorter latency to next interaction ($Z=-4.83$, $p<0.0001$), while time since target introduction predicted longer latency (Z=5.80, $p<0.0001$), as expected and consistent with cell body findings. In contrast, the effect for cell bodies in novel-object manipulation could not be found in projections to NAc (peak Ca^{2+} effect: Z=0.003, p=0.99; time elapsed effect: Z=0.48, p=0.64). Causal mediation analysis found strong direct effects for the VTA-NAc projection in social interaction (Fig 6F; 68.2% average direct effect, 31.8% average indirect effect mediated by time elapsed; both $p<0.0001$), similar to cell body results, with no significant direct or mediation effects for the novel object.

We sought to capitalize on this ability to track projection activity during behavior by probing in greater detail the encoding of specific behaviors by the VTA projection to NAc (in comparison with activity in VTA cell bodies) using multifactorial high-resolution quantitative behavioral assessment. We first employed an automated peak-finding algorithm (Methods) to detect all Ca^{2+} peaks throughout the 5-min testing period, blind to mouse behaviors, for social and novel object conditions during both VTA cell body and +6 projection recordings. Next we automatically segmented video clips centered (+/− 1 s) around the time of each Ca^{2+} peak, and scored video segments for interaction, approach, withdrawal, ambulation, grooming, rest, burrowing, rearing, and head extension (Methods). Based on results for Ca^{2+} peak size, decay profile, signal distribution, and causal mediation analyses above, we hypothesized that for social behavior, the % total Ca^{2+} peak activity representing target-relevant interaction behaviors would either remain the same or increase while recording from VTA-NAc projections compared to cell bodies (Fig. 6), and decrease for novel object behavior.

Area plots of all VTA-DA Ca^{2+} peak times subdivided by behavioral category (Fig. 7A,B), allowed direct comparison of total peak activity over time attributable to each category, including as a percent of total overall Ca^{2+} peak activity. In the social case, a larger proportion of total Ca^{2+} peak activity occurred during interaction for VTA-to-NAc projections than for cell bodies, further supporting the conclusion that this projection more selectively encodes social interaction than does the cell body signal (Fig. 7A). For novel object behavior, both cell bodies and projections poorly encoded approach or interaction (Fig. 7B); interestingly, while the VTA cell bodies seemed to strongly encode withdrawal from the object (as in Fig. 1H), the VTA-NAc projection only weakly encoded this specific behavior (Fig. 7B). Across the entire 5-min testing period, VTA-NAc projections showed a decreased proportion of Ca^{2+} peak activity (compared with VTA cell-body data) occurring during target-relevant behavior (accounted for by withdrawal) in the case of novel object but not social behavior (Fig. 7C,D). These data together support the conclusion that VTA-NAc projection activity represents a signal with specific importance to social behavior relative to object interactions.

Necessity and sufficiency of NAc D1R activity for social behavior modulation

To assess the final mechanistic step in this projection, we tested social-modulatory effects of postsynaptic cells and receptors in NAc. Most NAc cells are medium spiny neurons (MSNs), which can be divided into two broad categories defined by the type of DA receptor expressed (D1R or D2R, which couple to G_s and G_i signaling pathways, respectively; Beaulieu and Gainetdinov, 2011) with different roles in modulating reward; Lobo and

Nestler, 2011)). To determine which DA receptor could be involved in mediating effects of VTA stimulation, we infused D1- or D2-specific antagonists (SCH23390 and raclopride, respectively) into NAc prior to optical stimulation in social interaction (Fig. 8A). Infusion of D1R but not D2R antagonist into NAc attenuated the pro-social effect of light but not baseline levels of interaction (Fig. 8B and Fig. S5; n=15, LME model, t_{18}=2.29, p=0.035), indicating that DA signaling through D1Rs in NAc is necessary for mediating the social behavior increase elicited by VTA-DA neuron stimulation.

To test the sufficiency of D1R–expressing MSNs in social behavior with temporal precision, we sought to develop an engineered D1R that could be acutely controlled with light in behavior. We employed the OptoXR approach (Airan et al., 2009) to engineer direct optical control of D1R–mediated G_s signaling by replacing the intracellular loops of rhodopsin with those of D1R to form a chimeric Opto-D1 (Fig. 8C, Fig. S5). In HEK cells expressing the Opto-D1-eYFP fusion construct, selective upregulation of cAMP (G_s) but not IP3 (G_q) or cGMP (G_t) signaling pathways was driven by light, as anticipated (Fig. 8D, n=3, 4 readings each, unpaired t-test, p=0.002).

To fully leverage the specificity of sufficiency testing with Opto-D1, it would be ideal to transduce only cells that normally express D1R. We therefore next injected a Cre-dependent AAV virus carrying Opto-D1 into NAc of D1R (Drd1::Cre) transgenic mice to restrict expression to D1R MSNs (Fig. 8E). 473 nm light under these conditions was sufficient to increase social interaction (Fig. 9F, n=10 Opto-D1, n=10 eYFP, LME model, t_{18}=2.64, p=0.018) without affecting locomotion or novel object investigation (Fig. S5; Wilcoxon signed rank test, p=0.52, 0.40, respectively). Optrode recordings of Opto-D1 effects in NAc revealed ~3-fold light-increased multiunit activity (Fig. 8G–I; Wilcoxon signed rank test, p=0.01). Interestingly, the magnitude and direction of this D1R–mediated change in NAc spiking was consistent with the increase in NAc activity observed during natural social interaction as well as optogenetic VTA activation (Fig. 5). However, these data do not demonstrate that such an increase in spiking could suffice to drive increased social behavior; indeed D1R signaling could also affect many distinct aspects of cellular physiology and biochemistry. Therefore, as a final test of whether evoked increases in activity of NAc D1 cells could suffice to drive social interaction, we injected DIO-ChR2 AAV into NAc of D1R::Cre mice (Fig. 8J). Direct stimulation of firing in NAc D1 cells was indeed sufficient to produce a significant increase in social interaction compared to controls (Fig. 8K, n=6, LME model, t_{11}=2.26, p=0.039).

DISCUSSION

Here we have developed and applied fiber photometry, for direct measurement of a previously-inaccessible variable in neuroscience: the activity of specified neuronal afferents projecting to a particular downstream target during behavior. Using this method, we have found that an increase in activity in VTA DA neurons, especially in their projections to the NAc, predicts social interaction in freely-behaving mice. Fiber photometry can be used together with optogenetics to determine causal dynamics in both cell bodies and projections underlying complex behavior.

This ability to directly measure activity of projections between brain regions provides a new source of data on dynamics of information flow (Deisseroth, 2014). In network modeling, groups of neurons with similar projection patterns can be modeled as nodes in a network, and projections to downstream regions represented as directed links (Bullmore and Sporns, 2009). In simplified projection-based network dynamics terminology, each link from region i to a downstream region j can be modeled as providing a time-varying input $i \rightarrow j(t)$, which acting through a separate aggregate synaptic strength parameter $w_{ij}(t)$, defines the net influence of that projection from the neurons in region i onto those in region j at time t contributing to the aggregate postsynaptic response $j(t)$. Fiber photometry of projections now allows for the first time observation of these time varying inputs $i \rightarrow j(t)$ (independent of $w_{ij}(t)$ *and* $j(t)$), that represent the endogenous dynamics specific to one projection in the brain that can be thought of as the time-varying 'traffic' over the targeted link $i \rightarrow j$. It is worth noting that although the local field potential (LFP) can reflect synaptic input in a region (Linden et al., 2011), spontaneous LFP signals represent aggregate local readouts that cannot provide information on a specific projection from one brain region to another; moreover, even evoked LFP signals, in which an upstream brain region is stimulated, cannot report the native activity of a specific projection during behavior, nor do such electrically-evoked signals provide for specific recruitment of a genetically and topologically defined projection. To our knowledge this fundamental network parameter $i \rightarrow j(t)$ has not been accessible, and may define a key new measurement for dynamical network modeling.

Indeed, this kind of parameter appears especially predictive in behavior (Fig. 6). Moreover, projection-specific activity is also particularly important for causal elicitation of complex behaviors, as found here and elsewhere (reviewed in Deisseroth, 2014). Optogenetic enhancement of phasic activity in VTA-DA somata increased social behavior (concordant with the fiber photometry data and confirming that these neurons are causally involved in driving social interaction), but it is the projections to NAc and not other downstream regions such as PFC that predict and mediate this effect. Projection-specific optogenetic manipulations complement specificity of fiber photometry by enabling control of the corresponding dynamics $i \rightarrow j(t)$. Along with development and application of Opto-D1R enabling causal identification of postsynaptic NAc D1 MSNs regulating social behavior, these results demonstrate integrative value of complementary optical techniques in causally mapping specific projections and postsynaptic targets within neural circuitry.

Our observation that VTA DA neuron activity is causally involved in bidirectional modulation of same-sex social interaction supports prior pharmacological studies implicating DA in affiliative behaviors (Aragona et al., 2006; Curtis and Wang, 2005; Gingrich et al., 2000; Liu and Wang, 2003), though it had been previously difficult to determine the precise site and mechanism of action of DA as receptors are expressed postsynaptically as well as presynaptically on VTA terminals (Benoit-Marand et al., 2001; Palij et al., 1990) and pharmacological agents could exert behavioral effects either by enhancing DA signaling downstream or by dampening VTA activity via inhibitory autoreceptors. Additionally, NAc-projecting VTA neurons co-release glutamate (Stuber et al., 2010), and DA pharmacological manipulations do not typically capture this synergy present in endogenous VTA activity. The findings presented here illuminate not the role of a specific neurotransmitter but rather the circuit elements and dynamics in modulation of social behavior, defining relevant projections as well as pre- and post-synaptic cell types in mesolimbic circuitry.

An increase in NAc spiking occurred when animals chose to explore the social target, and two distinct pro-social optogenetic manipulations (VTA ChR2 and NAc Opto-D1 stimulation) at different steps in the putative circuit each increased NAc multiunit activity. These results are consistent with *in vivo* recordings showing increased NAc activity associated with reward-related behaviors, as well as studies implicating D1Rs in enhancing activity of MSNs (Lobo and Nestler, 2011; Moratalla et al., 1996). While the effects of DA on excitability are complex and depend on glutamatergic tone in NAc, activation of D1Rs is generally associated with increasing excitability of MSNs and activation of D2Rs is thought to decrease MSN excitability (Lobo and Nestler, 2011; Perez et al., 2006; Podda et al., 2010). Our results are also concordant with previous reports implicating D1 MSNs in enhancing the effects of rewarding stimuli (Lobo and Nestler, 2011). Mice display appetitive responses to same-sex social interaction even before reaching sexual maturity (Panksepp et al., 2007; Panksepp and Lahvis, 2007), and it may be that this natural reward can be provided or reinforced just as stimulating D1 MSNs drives animals to seek conditioned rewards (Lobo et al., 2010).

Here we have taken steps toward facilitating circuit-level understanding of the neural basis of complex behaviors, by addressing the roles of specific pre- and post-synaptic cell types defined by genetic and projection profile, and by providing a window into a fundamental network property (the direct real-time input from one brain region into another during behavior) with fiber photometry. In defining multiple components along an extended circuit regulating social behavior, we have explored the significance of specific cells, projections, and targets, rather than individual neurotransmitters. This approach may suggest circuit-based targets for further research into impaired social interaction and other neuropsychiatric disease-related symptoms, and may be generally applicable for investigation of specific circuit elements in mammalian behavior.

EXPERIMENTAL PROCEDURES

Animals

Adult female mice (aged 8 weeks at the start of experimental procedures) were used for all behavioral experiments. Mice were housed on a reverse 12 hr light/dark cycle and given food and water *ad libitum*. All animals were group housed except those implanted with chronic bundle electrodes. Estrous cycle stage was not examined as a factor in these studies. All experimental protocols were approved by the Stanford University IACUC following the National Institutes of Health guidelines for the Care and Use of Laboratory Animals.

Viral constructs

To achieve cell type specific opsin expression in Cre driver lines, we cloned the GCaMP5g, ChR2(H134R), eNpHR3.0, and Opto-D1 genes into the double-floxed inverted open reading frame plasmid pAAV-EF1α-DIO-ChR2-YFP-WPRE (Sohal et al., 2009). The WGA-Cre construct was expressed in the plasmid pAAV-EF1α-mCherry-IRES-WGA-Cre.

Behavioral testing

All tests were performed during the dark phase and animals were acclimated to the behavior room for at least 1 hr before testing. A 3 m long fiberoptic patchcord (Doric Lenses) was connected to the chronically implanted optical fiber with a zirconia sheath and suspended above the behavioral testing environment to allow animals to move freely during stimulation. The patchcord was connected to a 473 nm solid-state laser diode (OEM Laser Systems) with an FC/PC adapter. A Master-8 pulse stimulator (A.M.P.I., Jerusalem, Israel) controlled laser output. Phasic stimulation of VTA cell bodies and axon terminals consisted of 30 Hz bursts of 8 5-ms pulses of 473 nm light delivered every 5 sec at a light power output of 10 mW from the tip of the optical fiber. Activating light pulses for Opto-D1 consisted of continuous 473 nm light at 5 mW, and 591 nm continuous light at 1 mW for eNpHR3.0. For detailed descriptions of behavioral assays refer to the Supplementary Methods.

Fiber photometry

The fiber photometry system used a 473 nm diode laser (Omicron Luxx) that was chopped at 400 Hz, reflected off a dichroic (Semrock, FF495), and coupled into a 400 um 0.48 NA optical fiber using a 40× 0.65 NA microscope objective (Olympus) and fiber launch (Thorlabs). The laser intensity at the interface between the fiber tip and the animal ranged from 1.8–1.9 mW (but was constant across trials that were compared side by side). GCaMP fluorescence collected by the objective and transmitted by the dichroic was focused through a bandpass filter (Semrock, FF01–520/35) onto a NewFocus 2151 femtowatt silicon photoreceiver (Newport, DC Low mode), the output of which was directed through a lock-in amplifier (SR810 DSP, Stanford Research Systems, 3 ms time constant), digitized using a LabJack DAQ, and recorded by custom Python software. Signals were collected at a sampling frequency of 250 Hz.

Statistical analysis

For behavioral experiments, all binary comparisons were tested using nonparametric Wilcoxon rank-sum tests (paired or unpaired as appropriate), while hypotheses involving more than two group means were tested using linear contrasts in a linear mixed effects (LME) model. Electrophysiological data was fit by block bootstrapping 1000 times, applying a scaled adaptive nonparametric smoother (“akj” in R package “quantreg”) to each of the bootstrap replicates, allowing the calculation of 95% confidence intervals for the mean firing rate over time while adaptively allowing for sharp changes in firing rate. Kaplan-Meier estimates were used to compare latency to interact for the social and novel-object interaction behavior. For regressions of the latency to engage in social and novel-object interactions onto peak Ca^{2+} recording values we used survival regression (‘survreg’ in R’s ‘survival’ library). Causal mediation analyses were carried out using the ‘mediation’ library in R. For a more detailed description of these tests see Supplementary Methods.

NIH-PA Author Manuscript

NIH-PA Author Manuscript

Supplementary Material

Refer to Web version on PubMed Central for supplementary material.

Acknowledgments

We thank the entire Deisseroth lab for helpful discussions, and T. Jardetzky for use of a Biotek Synergy4 plate reader. L.A.G. is supported by a Stanford Bio-X Fellowship. L.G. is supported by NSF 0801700. L.E.F. is supported by the Stanford Medical Scientist Training Program. K.D. is supported by the Simons Foundation Autism Research Initiative, a Conte Center grant from NIMH, and NIDA, DARPA, the Gatsby Charitable Foundation, James Doty and the CCARE center at Stanford, the Stanford Institute for Neuroinnovation and Translational Neurosciences, and the Wiegers Family Fund. RCM and SL were supported by a grant from the Simons Foundation Autism Research Initiative and a Conte Center grant from NIMH. All optogenetic tools and methods described are distributed and supported freely (www.optogenetics.org).

REFERENCES

Adamantidis AR, Tsai HC, Boutrel B, Zhang F, Stuber GD, Budygin EA, Tourino C, Bonci A, Deisseroth K, de Lecea L. Optogenetic interrogation of dopaminergic modulation of the multiple phases of reward-seeking behavior. J Neurosci. 2011; 31:10829–10835. [PubMed: 21795535]

Airan RD, Thompson KR, Fenno LE, Bernstein H, Deisseroth K. Temporally precise in vivo control of intracellular signalling. Nature. 2009; 458:1025–1029. [PubMed: 19295515]

Akerboom J, et al. Optimization of a GCaMP calcium indicator for neural activity imaging. J Neurosci. 2012; 32:13819–13840. [PubMed: 23035093]

Aragona BJ, Liu Y, Yu YJ, Curtis JT, Detwiler JM, Insel TR, Wang Z. Nucleus accumbens dopamine differentially mediates the formation and maintenance of monogamous pair bonds. Nature neuroscience. 2006; 9:133–139.

Aravanis AM, Wang LP, Zhang F, Meltzer LA, Mogri MZ, Schneider MB, Deisseroth K. An optical neural interface: in vivo control of rodent motor cortex with integrated fiberoptic and optogenetic technology. Journal of neural engineering. 2007; 4:S143–S156. [PubMed: 17873414]

Balint E, Mezey S, Csillag A. Efferent connections of nucleus accumbens subdivisions of the domestic chicken (Gallus domesticus): an anterograde pathway tracing study. The Journal of comparative neurology. 2011; 519:2922–2953. [PubMed: 21618229]

Beaulieu JM, Gainetdinov RR. The physiology, signaling, and pharmacology of dopamine receptors. Pharmacological reviews. 2011; 63:182–217. [PubMed: 21303898]

Benoit-Marand M, Borrelli E, Gonon F. Inhibition of dopamine release via presynaptic D2 receptors: time course and functional characteristics in vivo. J Neurosci. 2001; 21:9134–9141. [PubMed: 11717346]

Brischoux F, Chakraborty S, Brierley DI, Ungless MA. Phasic excitation of dopamine neurons in ventral VTA by noxious stimuli. PNAS. 2009; 106:4894–4899. [PubMed: 19261850]

Budygin EA, Park J, Bass CE, Grinevich VP, Bonin KD, Wightman RM. Aversive stimulus differentially triggers subsecond dopamine release in reward regions. Neuroscience. 2012; 201:331–337. [PubMed: 22108611]

Bullmore E, Sporns O. Complex brain networks: graph theoretical analysis of structural and functional systems. Nature reviews Neuroscience. 2009; 10:186–198.

Chaudhury D, et al. Rapid regulation of depression-related behaviours by control of midbrain dopamine neurons. Nature. 2013; 493:532–536. [PubMed: 23235832]

Chen TW, et al. Ultrasensitive fluorescent proteins for imaging neuronal activity. Nature. 2013; 499:295–300. [PubMed: 23868258]

Cui G, Jun SB, Jin X, Pham MD, Vogel SS, Lovinger DM, Costa RM. Concurrent activation of striatal direct and indirect pathways during action initiation. Nature. 2013; 494:238–242. [PubMed: 23354054]

Curtis JT, Wang Z. Ventral tegmental area involvement in pair bonding in male prairie voles. Physiology & behavior. 2005; 86:338–346. [PubMed: 16165168]

Deisseroth K. Circuit dynamics of adaptive and maladaptive behaviour. Nature. 2014; 505:309–317. [PubMed: 24429629]

Dong Y, Li J, Zhang F, Li Y. Nociceptive afferents to the premotor neurons that send axons simultaneously to the facial and hypoglossal motoneurons by means of axon collaterals. PloS one. 2011; 6:e25615. [PubMed: 21980505]

Gingrich B, Liu Y, Cascio C, Wang Z, Insel TR. Dopamine D2 receptors in the nucleus accumbens are important for social attachment in female prairie voles (Microtus ochrogaster). Behavioral neuroscience. 2000; 114:173–183. [PubMed: 10718272]

Gradinaru V, Zhang F, Ramakrishnan C, Mattis J, Prakash R, Diester I, Goshen I, Thompson KR, Deisseroth K. Molecular and cellular approaches for diversifying and extending optogenetics. Cell. 2010; 141:154–165. [PubMed: 20303157]

Graybiel AM. The basal ganglia. Curr Biol. 2000; 10:R509–R511. [PubMed: 10899013]

Imai K, Keele L, Tingley D. A general approach to causal mediation analysis. Psychological methods. 2010; 15:309–334. [PubMed: 20954780]

Kalivas PW, Nakamura M. Neural systems for behavioral activation and reward. Current opinion in neurobiology. 1999; 9:223–227. [PubMed: 10322190]

Kravitz AV, Freeze BS, Parker PR, Kay K, Thwin MT, Deisseroth K, Kreitzer AC. Regulation of parkinsonian motor behaviours by optogenetic control of basal ganglia circuitry. Nature. 2010; 466:622–626. [PubMed: 20613723]

Lammel S, Hetzel A, Hackel O, Jones I, Liss B, Roeper J. Unique properties of mesoprefrontal neurons within a dual mesocorticolimbic dopamine system. Neuron. 2008; 57:760–773. [PubMed: 18341995]

Lammel S, Ion DI, Roeper J, Malenka RC. Projection-specific modulation of dopamine neuron synapses by aversive and rewarding stimuli. Neuron. 2011; 70:855–862. [PubMed: 21658580]

Lammel S, Lim BK, Ran C, Huang KW, Betley MJ, Tye KM, Deisseroth K, Malenka RC. Input-specific control of reward and aversion in the ventral tegmental area. Nature. 2012; 491:212–217. [PubMed: 23064228]

Leypold BG, Yu CR, Leinders-Zufall T, Kim MM, Zufall F, Axel R. Altered sexual and social behaviors in trp2 mutant mice. PNAS. 2002; 99:6376–6381. [PubMed: 11972034]

Linden H, Tetzlaff T, Potjans TC, Pettersen KH, Grun S, Diesmann M, Einevoll GT. Modeling the spatial reach of the LFP. Neuron. 2011; 72:859–872. [PubMed: 22153380]

Liu Y, Wang ZX. Nucleus accumbens oxytocin and dopamine interact to regulate pair bond formation in female prairie voles. Neuroscience. 2003; 121:537–544. [PubMed: 14568015]

Lobo MK, et al. Cell type-specific loss of BDNF signaling mimics optogenetic control of cocaine reward. Science. 2010; 330:385–390. [PubMed: 20947769]

Lobo MK, Nestler EJ. The striatal balancing act in drug addiction: distinct roles of direct and indirect pathway medium spiny neurons. Frontiers in neuroanatomy. 2011; 5:41. [PubMed: 21811439]

Lutcke H, Murayama M, Hahn T, Margolis DJ, Astori S, Zum Alten Borgloh SM, Gobel W, Yang Y, Tang W, Kugler S, et al. Optical recording of neuronal activity with a genetically-encoded calcium indicator in anesthetized and freely moving mice. Frontiers in neural circuits. 2010; 4:9. [PubMed: 20461230]

Mirenowicz J, Schultz W. Preferential activation of midbrain dopamine neurons by appetitive rather than aversive stimuli. Nature. 1996; 379:449–451. [PubMed: 8559249]

Moratalla R, Xu M, Tonegawa S, Graybiel AM. Cellular responses to psychomotor stimulant and neuroleptic drugs are abnormal in mice lacking the D1 dopamine receptor. PNAS. 1996; 93:14928–14933. [PubMed: 8962158]

Moy SS, Nadler JJ, Perez A, Barbaro RP, Johns JM, Magnuson TR, Piven J, Crawley JN. Sociability and preference for social novelty in five inbred strains: an approach to assess autistic-like behavior in mice. Genes, brain, and behavior. 2004; 3:287–302.

Palij P, Bull DR, Sheehan MJ, Millar J, Stamford J, Kruk ZL, Humphrey PP. Presynaptic regulation of dopamine release in corpus striatum monitored in vitro in real time by fast cyclic voltammetry. Brain research. 1990; 509:172–174. [PubMed: 2137719]

Panksepp JB, Jochman KA, Kim JU, Koy JJ, Wilson ED, Chen Q, Wilson CR, Lahvis GP. Affiliative behavior, ultrasonic communication and social reward are influenced by genetic variation in adolescent mice. PloS one. 2007; 2:e351. [PubMed: 17406675]

Panksepp JB, Lahvis GP. Social reward among juvenile mice. Genes, brain, and behavior. 2007; 6:661–671.

Perez MF, White FJ, Hu XT. Dopamine D(2) receptor modulation of K(+) channel activity regulates excitability of nucleus accumbens neurons at different membrane potentials. Journal of neurophysiology. 2006; 96:2217–2228. [PubMed: 16885524]

Podda MV, Riccardi E, D'Ascenzo M, Azzena GB, Grassi C. Dopamine D1-like receptor activation depolarizes medium spiny neurons of the mouse nucleus accumbens by inhibiting inwardly rectifying K+ currents through a cAMP-dependent protein kinase A-independent mechanism. Neuroscience. 2010; 167:678–690. [PubMed: 20211700]

Puglisi-Allegra S, Cabib S. Psychopharmacology of dopamine: the contribution of comparative studies in inbred strains of mice. Progress in neurobiology. 1997; 51:637–661. [PubMed: 9175160]

Robinson DL, Heien ML, Wightman RM. Frequency of dopamine concentration transients increases in dorsal and ventral striatum of male rats during introduction of conspecifics. J Neurosci. 2002; 22:10477–10486. [PubMed: 12451147]

Robinson DL, Zitzman DL, Smith KJ, Spear LP. Fast dopamine release events in the nucleus accumbens of early adolescent rats. Neuroscience. 2011; 176:296–307. [PubMed: 21182904]

Schulz K, Sydekum E, Krueppel R, Engelbrecht CJ, Schlegel F, Schroter A, Rudin M, Helmchen F. Simultaneous BOLD fMRI and fiber-optic calcium recording in rat neocortex. Nature methods. 2012; 9:597–602. [PubMed: 22561989]

Silva AJ, Ehninger D. Adult reversal of cognitive phenotypes in neurodevelopmental disorders. Journal of neurodevelopmental disorders. 2009; 1:150–157. [PubMed: 19812701]

Sohal VS, Zhang F, Yizhar O, Deisseroth K. Parvalbumin neurons and gamma rhythms enhance cortical circuit performance. Nature. 2009; 459:698–702. [PubMed: 19396159]

Stuber GD, Hnasko TS, Britt JP, Edwards RH, Bonci A. Dopaminergic terminals in the nucleus accumbens but not the dorsal striatum corelease glutamate. J Neurosci. 2010; 30:8229–8233. [PubMed: 20554874]

Tsai HC, Zhang F, Adamantidis A, Stuber GD, Bonci A, de Lecea L, Deisseroth K. Phasic firing in dopaminergic neurons is sufficient for behavioral conditioning. Science. 2009; 324:1080–1084. [PubMed: 19389999]

Tye KM, et al. Dopamine neurons modulate neural encoding and expression of depression-related behaviour. Nature. 2013; 493:537–541. [PubMed: 23235822]

Warden MR, Selimbeyoglu A, Mirzabekov JJ, Lo M, Thompson KR, Kim SY, Adhikari A, Tye KM, Frank LM, Deisseroth K. A prefrontal cortex-brainstem neuronal projection that controls response to behavioural challenge. Nature. 2012; 492:428–432. [PubMed: 23160494]

Winslow JT. Crawley, Jacqueline N., et al.Mouse social recognition and preference. Current protocols in neuroscience. 2003 Chapter 8, Unit 16.

Xu W, Sudhof TC. A neural circuit for memory specificity and generalization. Science. 2013; 339:1290–1295. [PubMed: 23493706]

Young LJ, Lim MM, Gingrich B, Insel TR. Cellular mechanisms of social attachment. Hormones and behavior. 2001; 40:133–138. [PubMed: 11534973]

Young LJ, Wang Z. The neurobiology of pair bonding. Nature neuroscience. 2004; 7:1048–1054.

Yuan K, Shih JY, Winer JA, Schreiner CE. Functional networks of parvalbumin-immunoreactive neurons in cat auditory cortex. J Neurosci. 2011; 31:13333–13342. [PubMed: 21917816]

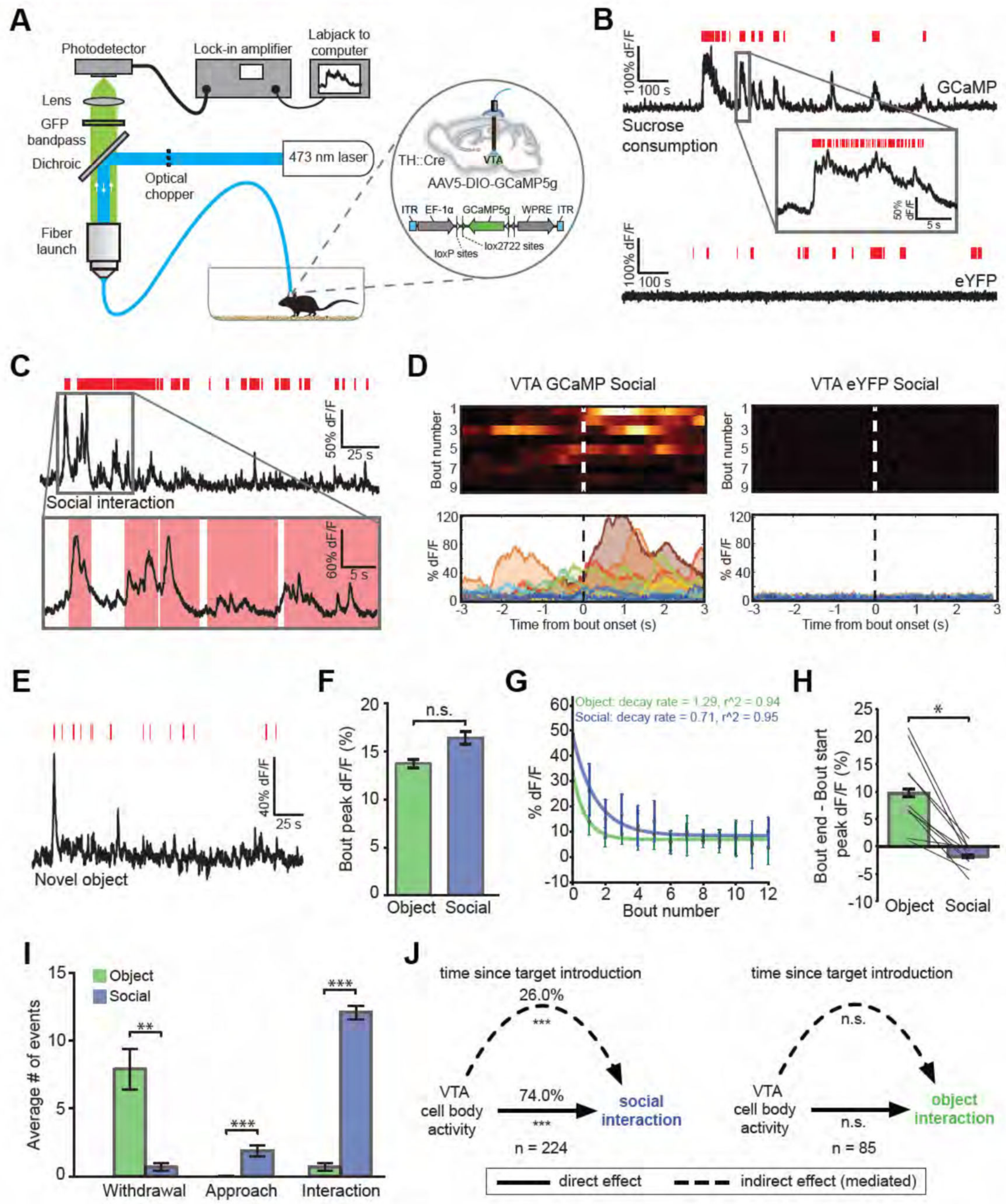

Figure 1. Fiber photometry of neural dynamics during social interaction

(A) Left: photometry setup. Light path for fluorescence excitation and emission is through a single 400μm fiberoptic implanted in VTA. Right: viral targeting of GCaMP5 to VTA-DA neurons. (B) Photometry traces from mice expressing eYFP (bottom) and GCaMP5.0 (top) in VTA during the sucrose lickometer test, showing robust increases in GCaMP fluorescence correlated with sucrose licking epochs (red dashes). dF/F represents change in fluorescence from median of the entire time-series. (C) Top: example trace of VTA-DA activity in social behavior. Red dashes: interaction bouts. Bottom: zoom-in of dashed interval relating VTA-DA GCaMP signal and social interaction (colored boxes). (D) Example heatmaps (top) and peri-event plots (bottom) aligned to start of interaction for mice expressing GCaMP (left) or eYFP (right). Heatmaps: warmer colors indicate higher fluorescence signal; peri-event plots: warmer colors represent earlier interaction bouts. (E) VTA-DA activity in novel object investigation. Red dashes: interaction bouts. (F) Average peak fluorescence over first ten interaction bouts (16.4% dF/F: social; 13.7% dF/F: novel object; n=10, Wilcoxon signed-rank test, p=0.5). (G) Signal changes across bouts: social (blue) and novel object (green). (H) Signal changes within bouts; novel object peak responses occur closer to interaction-bout end than do social peak responses (n=10 individual animals plotted, gray lines; difference of peaks over 0.5 s from bout-end and bout-start: −1.7% dF/F social vs. 9.7% dF/F novel object; Wilcoxon signed-rank test: p=0.0051). (I) Specific behaviors during 1 sec behavioral video clips centered around peak fluorescence within each bout. Peak during novel object investigation occurs predominantly in withdrawing from object (92%), while peak fluorescence during social interaction occurs in approach (14%) or active investigation (81%) (n=10 animals, 15 bouts/animal). (J) Directed-graph model of causal mediation analysis (Methods); while time-elapsed partially mediates effects of VTA-DA neuron activity on latency to social interaction only, the majority of effect was direct rather than mediated (74.0% average direct effect, 26.0% average indirect effect mediated by time elapsed; both p<0.0001). See also Figure S1.

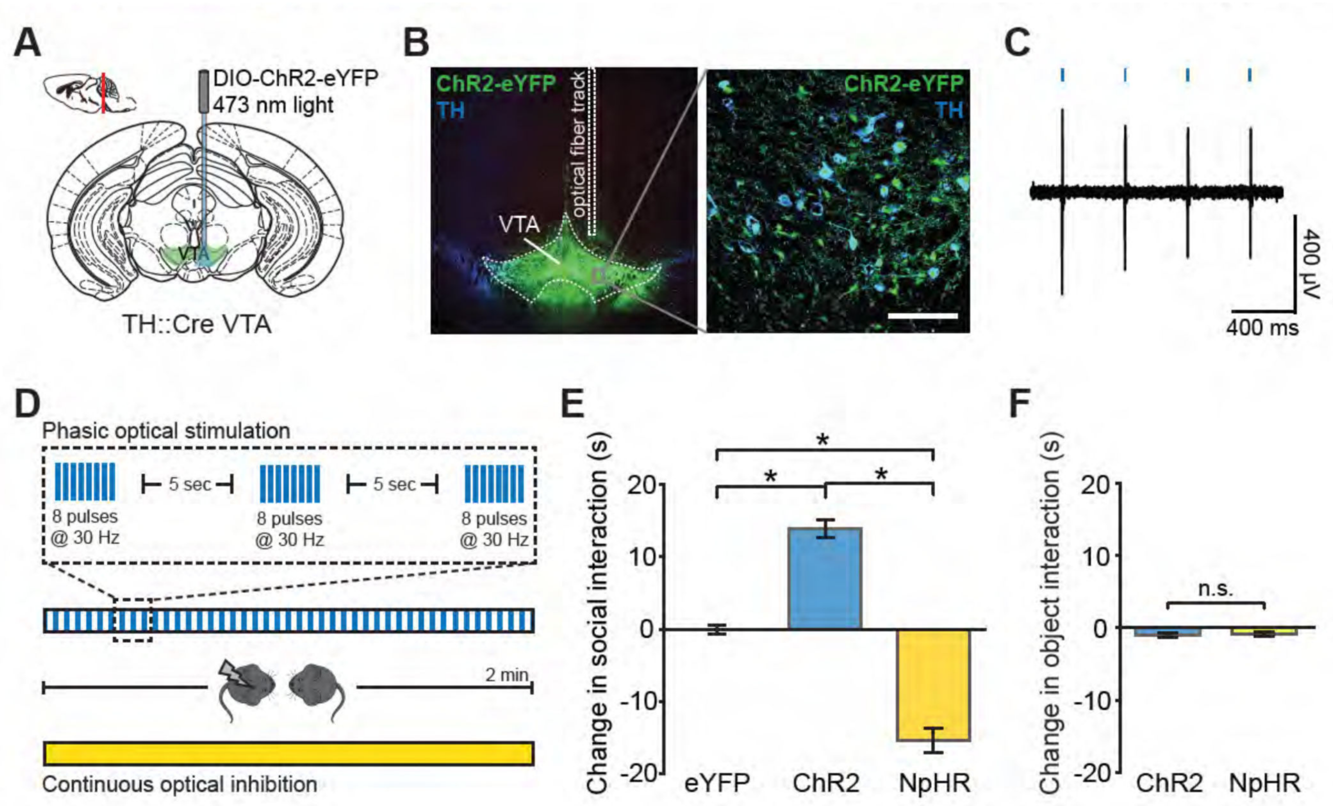

Figure 2. VTA modulation of social behavior

(A) Injection of AAV5-DIO-ChR2 into VTA of TH::Cre mice. (B) Confocal image: ChR2-eYFP expression in VTA, colocalization with TH (blue). Scale bar: 100 µm. (C) *In vivo* anesthetized recording of light-evoked spikes from TH::Cre mouse: ChR2 in VTA. (D) Optical stimulation parameters for home cage interaction. For excitation, 473nm light was delivered in 30 Hz bursts (8 pulses, 5 ms each) every 5 seconds. For inhibition, continuous 591nm light was delivered. (E) Summary of light-evoked changes in social interaction after bidirectional control of DA neurons. Phasic stimulation of VTA cell bodies increased social interaction compared to eYFP (n=17 ChR2 and n=18 eYFP, LME model, t_{57}=2.31, p=0.03), while inhibition of VTA cell bodies decreased interaction (n=10 eNpHR3.0 and n=15 eYFP, LME model, t_{57}=−2.09, p=0.04). (F) Neither stimulation nor inhibition of VTA cell bodies significantly affected novel object interaction (p>0.05). See also Figure S2.

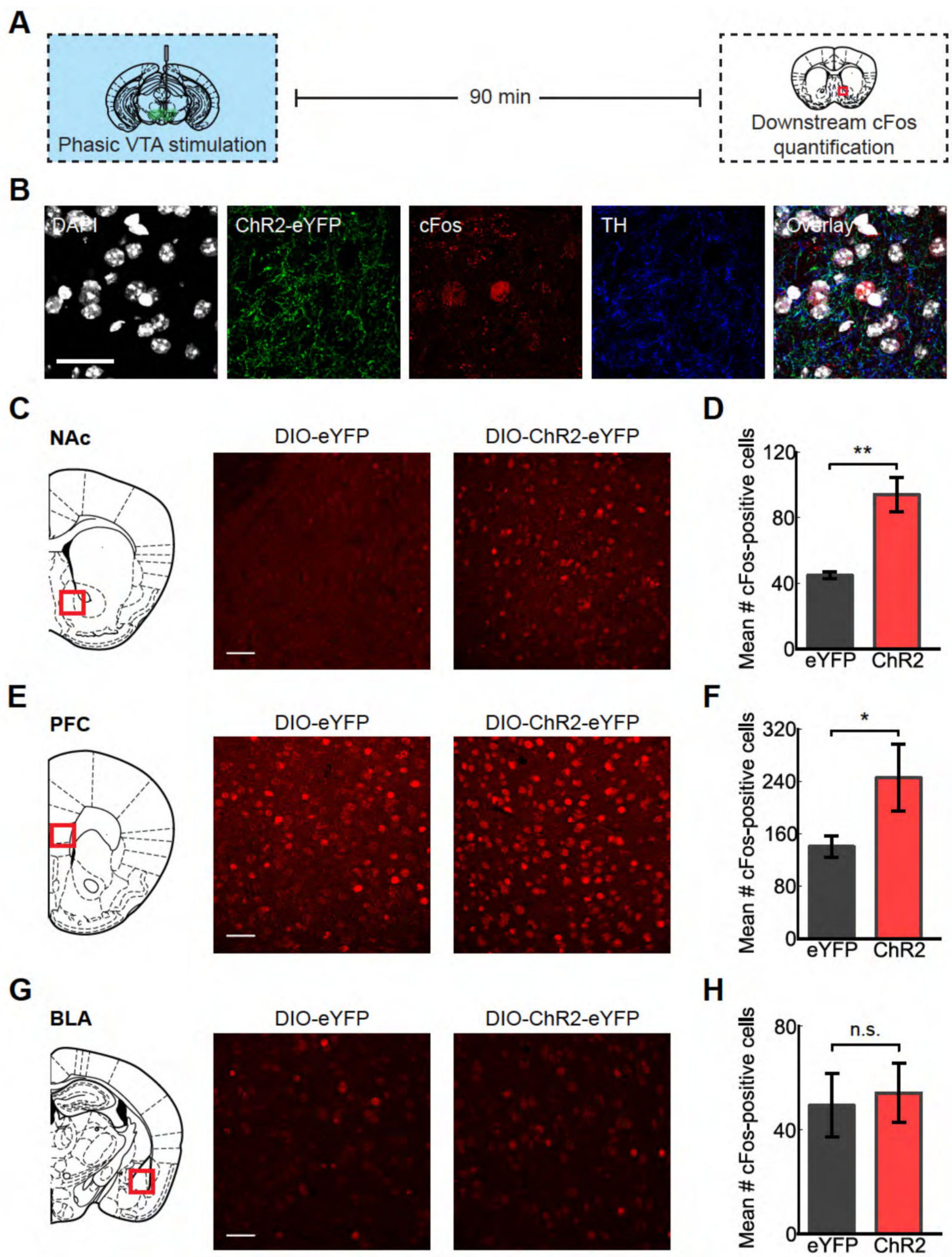

Figure 3. Downstream regions recruited by optogenetic VTA stimulation

(A) Animals were stimulated for 5 min (home-cage) and sacrificed 90 min later. (B) Confocal images: ChR2-eYFP in VTA-orginating fibers in NAc; induction of NAc cFos by VTA stimulation. White: DAPI nuclear stain, green: ChR2-eYFP, red: cFos, blue: anti-TH labeling of DA fibers. Scale bar: 25 μm. (C) Images of NAc medial shell from eYFP and ChR2 slices; increased cFos+ NAc cells in ChR2 brain following VTA stimulation. (D) cFos induction by VTA stimulation: NAc cFos increase in ChR2 compared to control (n=4 eYFP, n=4 ChR2; t-test, p=0.00006). (E) Images of PFC from eYFP control and ChR2 slices;

increased cFos+ PFC cells in the ChR2 brain following VTA stimulation. (F) cFos induction by VTA stimulation: PFC cFos increase in ChR2 compared to control (n=4 eYFP, n=3 ChR2; t-test, p=0.002). (G) Images of BLA from eYFP and ChR2 slices; no change in cFos+ PFC cells in the ChR2 brain following VTA stimulation. (H) BLA cFos induction by VTA stimulation; no difference between ChR2 and control (n=4 eYFP, n=4 ChR2; t-test, p=0.82).

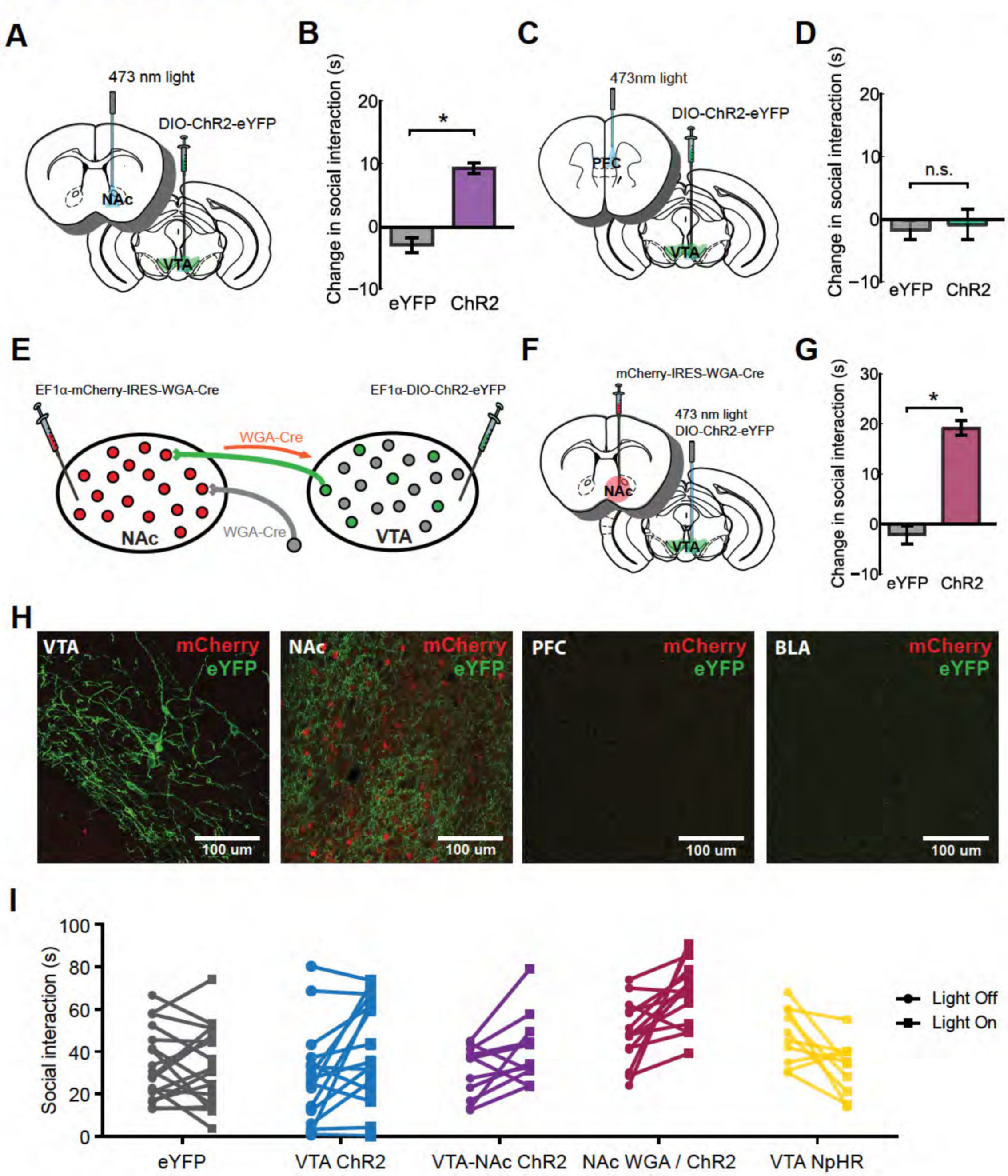

Figure 4. Projection-specific VTA control of social behavior

(A) ChR2 in VTA DA neurons and optical fiber implantation above NAc, targeting VTA-to-NAc projections. (B) Phasic stimulation of VTA-originating axons in NAc increased social interaction in ChR2 animals (purple) compared to controls (gray) (n=11 ChR2, n=12 eYFP; LME model, t_{30}=7.11, p=0.039). (C) ChR2 expression in VTA DA neurons and optical fiber implantation above PFC, targeting VTA-to-PFC projections. (D) Phasic stimulation of VTA-originating axons in PFC had no effect on social interaction in ChR2 animals (blue) or controls (gray) (n=7/group; LME model, t_{12}= 0.11, p=0.39). (E) Injection of mCherrylabeled WGA-Cre into NAc and Cre-dependent ChR2-eYFP into VTA of wild-type mice. WGA-Cre is trans-synaptically transported to all cells upstream of the NAc (orange arrow) but ChR2 expression is only activated in the subset of VTA neurons topologically defined by projections to medial NAc. (F) ChR2 in the subset of VTA neurons that project to medial NAc; optical fiber implantation above VTA. (G) Phasic stimulation of this subpopulation of VTA neurons increased social interaction in ChR2 animals (magenta) but not controls (gray) (n=14/group; LME model, t_{23}=2.53, p=0.02). (H) Sparse but strong ChR2-eYFP expression in VTA using this dual-virus system. ChR2-eYFP labels VTA fibers in medial NAc where WGA-Cre virus was injected, with negligible labeling of PFC or BLA fibers. Scale bars: 100 μm. (I) Summary of bidirectional effects of VTA interventions in individual animals. Consistency of pro-social effects increased with ChR2 projection specificity, and optical inhibition of VTA decreased social interaction. Gray: eYFP controls, blue: VTA DA cell body stimulation, purple: VTA-NAc axonal stimulation, magenta: WGA-Cre-isolated VTA-NAc projection, yellow: VTA DA cell body inhibition with eNpHR3.0. See also Figure S3.

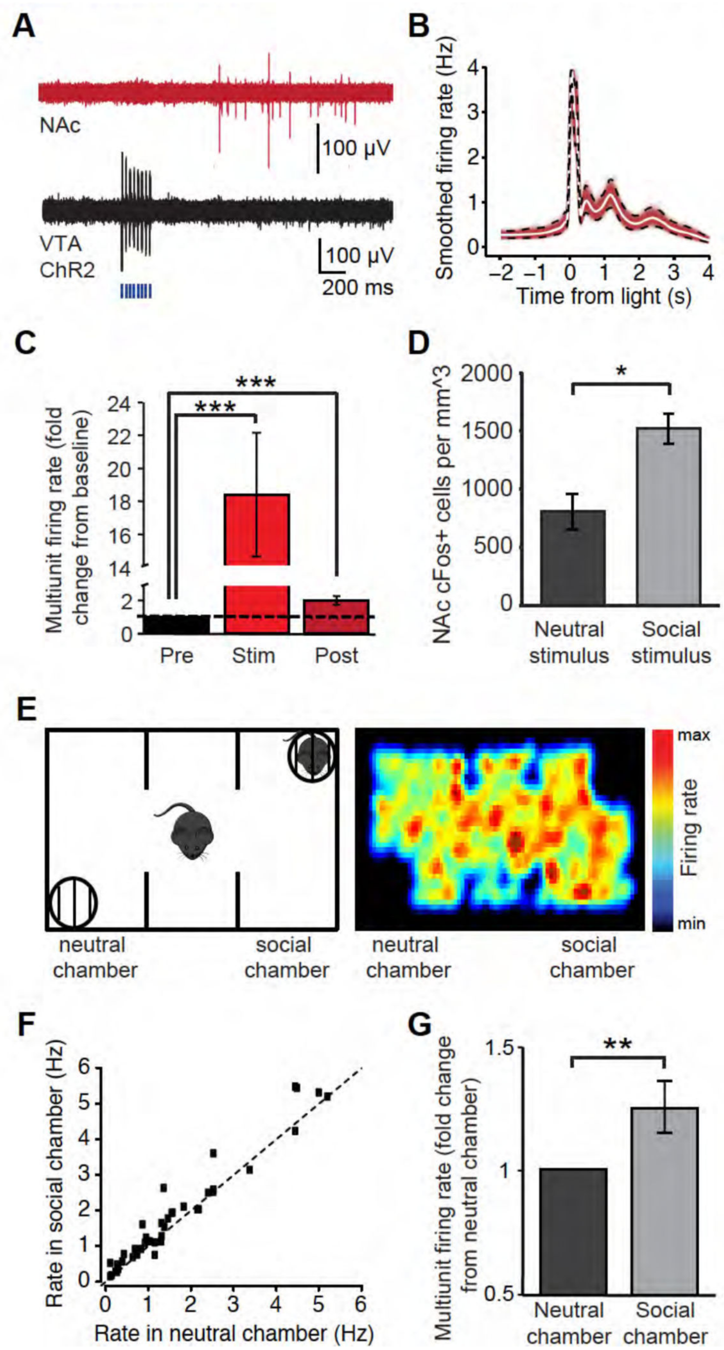

Figure 5. Electrophysiologic assessment in NAc of increased social behavior

(A) NAc activity (red) evoked by VTA stimulation (black). (B) PSTH: light-evoked increase in NAc firing with one burst of VTA stimulation. (C) Summary graph from (B): increase in NAc firing during/following a burst of light to VTA (Wilcoxon signed-rank test, p<0.001). (D) Increase in NAc cFos in un-implanted mice; social vs. neutral stimulus (wire mesh cup) (5 min, n=3/group; t-test, p=0.03). (E) Left: NAc activity in a freely moving animal exploring neutral and social environments. Right: heat map: firing rate of NAc neurons higher in social compared to neutral chamber. Warmer colors: higher firing rate. (F)

NIH-PA Author Manuscript

NIH-PA Author Manuscript

Correlation of firing rate in social vs. neutral chamber for each multiunit recording site: note greater activity in social chamber (black dots: individual multiunit recording sites; dashed line: unity). (G) NAc spiking higher in social environment (Wilcoxon signed-rank test, p=0.025). See also Figure S4.

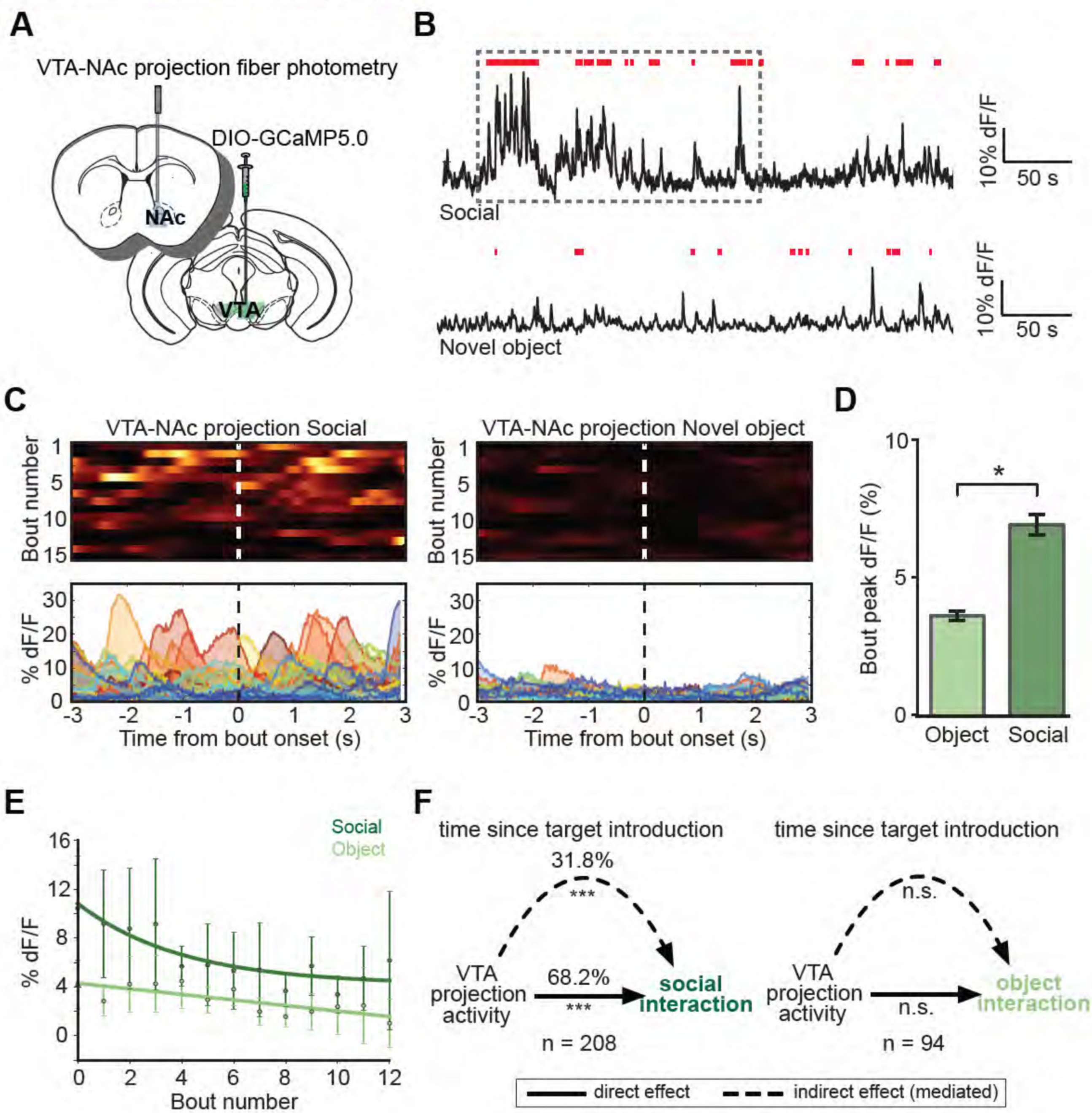

Figure 6. Fiber photometry assessment of DA projection activity in NAc during social interaction

(A) Fiber photometry of VTA projections in NAc. (B) VTA projection activity during social (top) and novel object investigation (bottom; interaction bouts in red). (C) Heatmaps (top) and peri-event plots (bottom) of NAc projection fluorescence aligned to start of interaction bout for social or novel object investigation. For heatmaps, warmer colors indicate higher fluorescence signal; peri-event plots: warmer colors indicate earlier interaction bouts. (D) NAc projections largely recapitulate social signals in VTA, with lower response to novel object (n=11, Wilcoxon signed-rank test, mean peak fluorescence: 6.9% dF/F social, 3.6%

dF/F novel object, $p=0.016$). (E) Decay of NAc projection signal across bouts. Decay in signal during social behavior is slower in projections than cell bodies. Social decay rate=0.2491, $r^2=0.8$; Object decay rate=0.0012, $r^2=0.6$. (F) Directed graphical model of causal mediation analysis; while time elapsed partially mediated effects of VTA-NAc projection activity on latency to social interaction, the major effect was direct (68.2% average direct effect, 31.8% average indirect effect mediated by time elapsed; both $p<0.0001$). No significant direct or indirect effects of VTA-NAc projection activity on latency to interact were observed in novel object investigation.

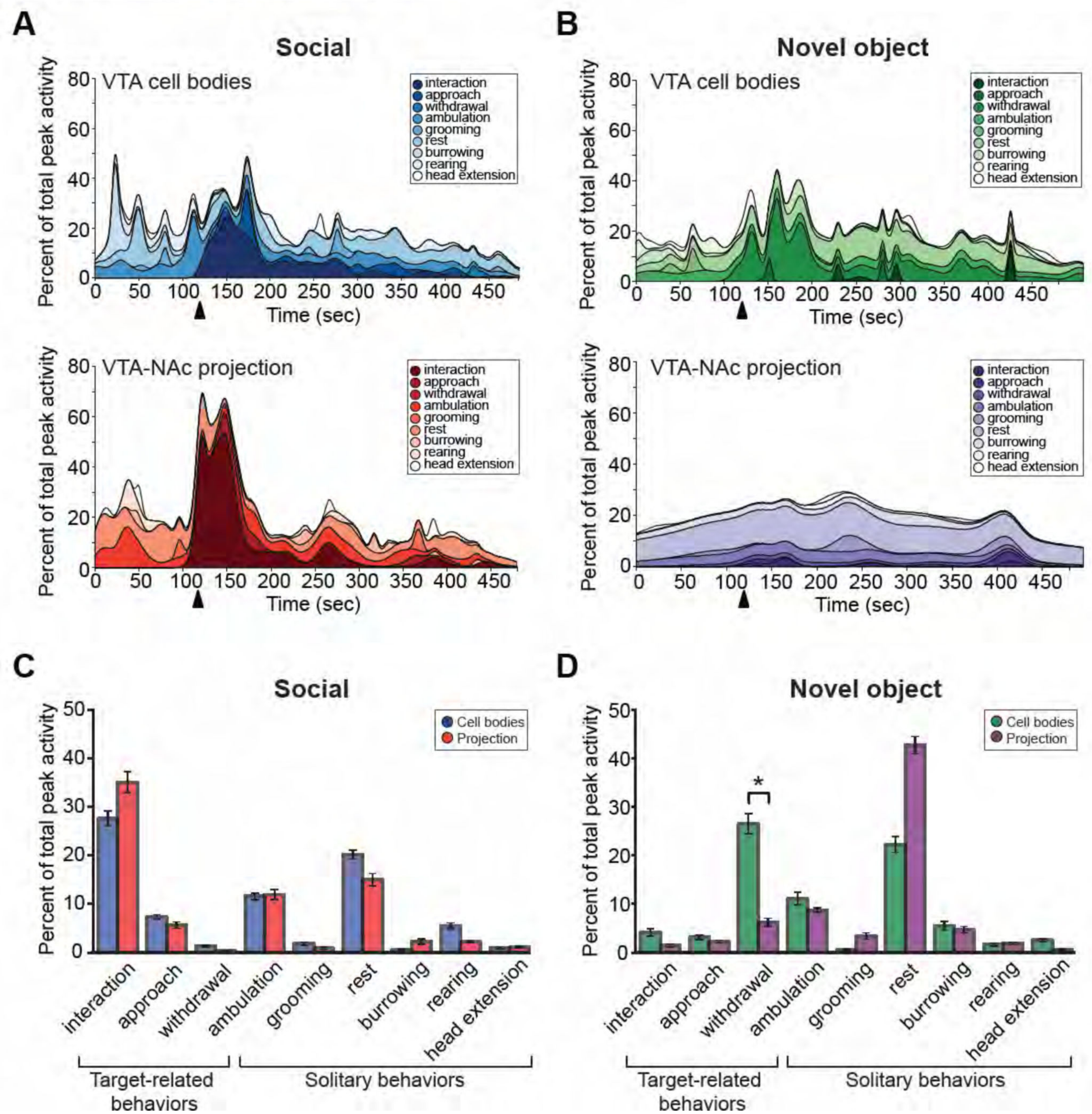

Figure 7. VTA-NAc projection activity encodes social interaction

(A) Area plots, smoothed behavioral score: %total Ca^{2+} peaks representing specific social target-related and solitary behaviors during VTA cell body (top) and VTA-NAc projection (bottom) fiber photometry (5 min; n=10 and n=11 mice, respectively). Arrows: target introduction. (B) Area plots, smoothed behavioral score: %total Ca^{2+} peaks representing specific novel object-related and solitary behaviors during VTA cell body (top) and VTA-NAc projection (bottom) fiber photometry (5 min; n=10 and n=11 mice, respectively). (C) Summary of data from (A): average %total Ca^{2+} peaks in target-related and solitary behaviors while recording VTA cell bodies (blue) and VTA-NAc projections (red) in the social assay. Note encoding of social interaction by VTA cell body and VTA-NAc projection activity. (D) Summary of data from (B): average %total Ca^{2+} peaks in target-related and solitary behaviors while recording VTA cell bodies (green) and VTA-NAc projections (purple) in the novel object assay. After correcting for multiple comparisons, only VTA-NAc projection activity at withdrawal represented a significantly smaller proportion of total peak activity compared to VTA cell body activity (two-sample permutation t-test; p=0.034 (Holm-corrected), n=11), suggesting a specific reduction of object-related activity in VTA-NAc projections (the largest contributor to activity peaks in the novel object VTA cell body assay).

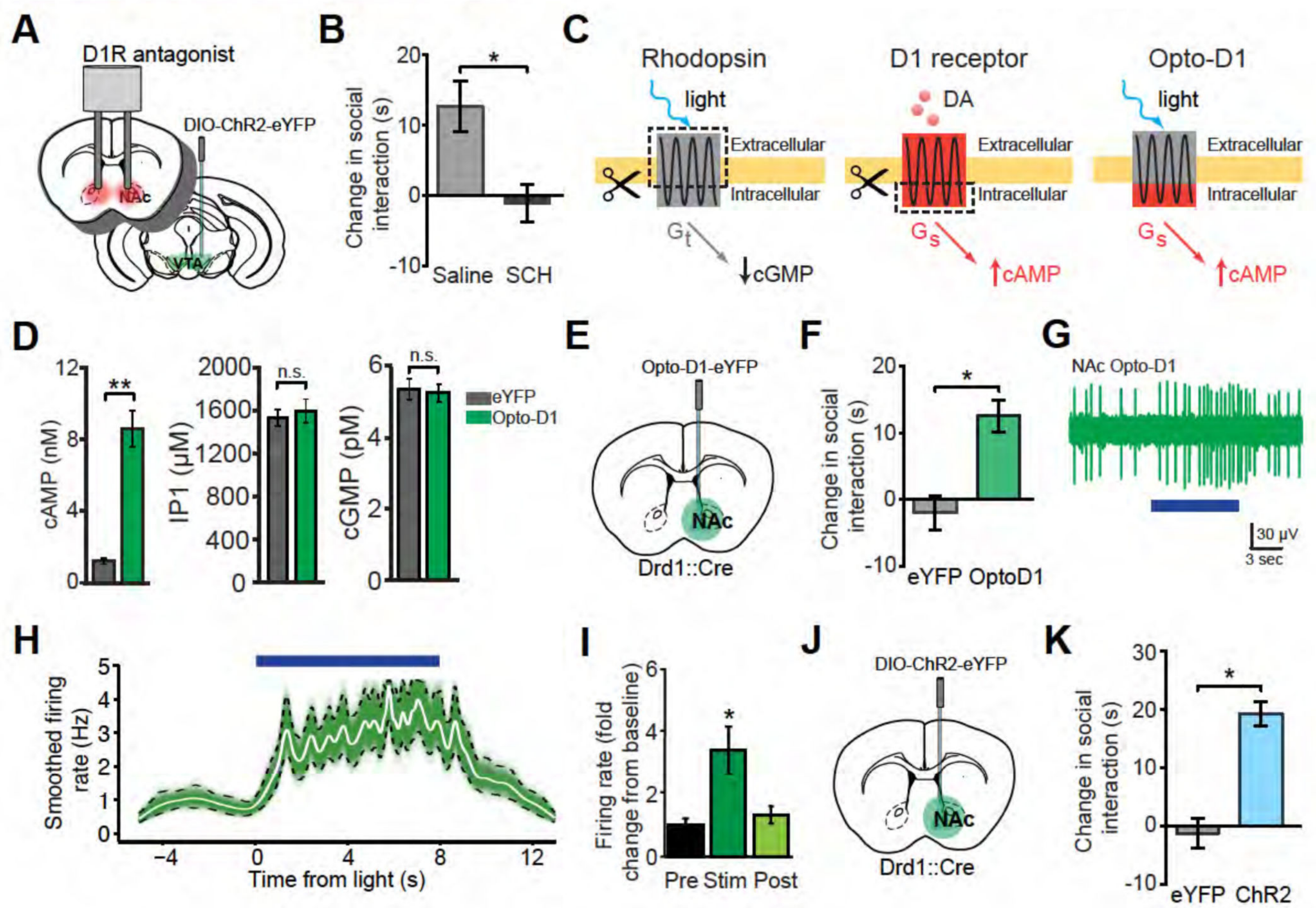

Figure 8. Postsynaptic NAc D1 cells and receptors in natural and VTA stimulation-driven social behavior

(A) Infusion of D1 receptor (D1R) antagonist SCH23390 into NAc prior to VTA stimulation during social interaction. (B) Compared to control saline infusion, D1R antagonism attenuated light-evoked increases in social behavior (n=15, LME model, t_{18}=2.29, p=0.035). (C) Opto-D1 design: replacing intracellular loops of rhodopsin with those of D1R. (D) *In vitro* GPCR signaling assays show selective upregulation of cAMP but not IP3 or cGMP pathways by Opto-D1 (n=3 samples, 4 readings each, unpaired t-test, p=0.002). (E) Infusion of DIO-Opto-D1 virus into NAc of Drd1::Cre mice for selective expression in D1R+ NAc cells. (F) Illumination of Opto-D1 in NAc D1 cells with continuous 473 nm light increased social interaction compared to eYFP controls (n=10 per group, LME model, t_{18}=2.64, p=0.018). (G) Example recording of NAc activity with Opto-D1 activation. (H) PSTH: light-evoked increase in NAc firing with Opto-D1. (I) Summary graph from (H): increase in NAc firing during activation of Opto-D1 (Wilcoxon signed-rank test, p=0.01). (J) Infusion of DIO-ChR2 into NAc of Drd1::Cre mice. (K) Tonic 10 Hz stimulation of NAc D1R cells increased social interaction (n=6, LME model, t_{11}=2.26, p=0.039). See also Figure S5.